

# Forecasting the Tropical Cyclone Genesis over the Northwest Pacific through Identifying the Causal Factors in Cyclone–Climate Interactions

CHENGZU BAI, REN ZHANG, AND SENLIANG BAO

*Research Center of Ocean Environment Numerical Simulation, Institute of Meteorology and Oceanography, National University of Defense Technology, and Collaborative Innovation Center on Forecast Meteorological Disaster Warning and Assessment, Nanjing University of Information Science and Technology, Nanjing, China*

X. SAN LIANG

*Nanjing Institute of Meteorology, Nanjing, China*

WENBO GUO

*China Satellite Maritime Tracking and Control Department, Jiangyin, China*

(Manuscript received 16 June 2017, in final form 16 November 2017)

## ABSTRACT

How to extract the causal relations in climate–cyclone interactions is an important problem in atmospheric science. Traditionally, the most commonly used research methodology in this field is time-delayed correlation analysis. This may be not appropriate, since a correlation cannot imply causality, as it lacks the needed asymmetry or directedness between dynamical events. This study introduces a recently developed and very concise but rigorous formula—that is, a formula for information flow (IF)—to fulfill the purpose. A new way to normalize the IF is proposed and then the normalized IF (NIF) is used to detect the causal relation between the tropical cyclone (TC) genesis over the western North Pacific (WNP) and a variety of climate modes. It is shown that El Niño–Southern Oscillation and Pacific decadal oscillation are the dominant factors that modulate the WNP TC genesis. The western Pacific subtropical high and the monsoon trough are also playing important roles in affecting the TCs in the western and eastern regions of the WNP, respectively. With these selected climate indices as predictors, a method of fuzzy graph evolved from a nonparametric Bayesian process (BNP-FG), which is capable of handling situations with insufficient samples, is employed to perform a seasonal TC forecast. A forecast with the classic Poisson regression is also conducted for comparison. The BNP-FG model and the causality analysis are found to provide a satisfactory estimation of the number of TC genesis observed in recent years. Considering its generality, it is expected to be applicable in other climate-related predictions.

## 1. Introduction

In predicting the interannual variability of tropical cyclone (TC; see [appendix A](#) for a glossary of the acronyms) geneses over the western North Pacific (WNP), there are two outstanding problems that have caught wide attention. The first problem is unraveling the causal relation between various climate factors and the

WNP TC genesis, and the other problem is how to forecast the TC genesis. Regarding the first problem, there have been many studies on cyclone–climate interactions over the WNP. For example, [Wang and Chan \(2002\)](#) and [Zhan et al. \(2011\)](#) found that El Niño–Southern Oscillation (ENSO) contributes to both the east–west shift of the WNP TC birth places and the TC intensity, because ENSO plays a vital role in the interannual variability of the barotropic energy conversion in the region, which leads to change in meridional shear of the large-scale zonal wind, and hence induces more intense TCs in El Niño years. Motivated by [Gray \(1998\)](#), [Chia and Ropelewski \(2002\)](#) observed that the interannual modulation of the WNP TC genesis is related to the west Pacific sea surface temperature (SST), the

---

Supplemental information related to this paper is available at the Journals Online website: <https://doi.org/10.1175/JTECH-D-17-0109.s1>.

---

Corresponding author: R. Zhang, [zrpaper@163.com](mailto:zrpaper@163.com)

DOI: 10.1175/JTECH-D-17-0109.1

© 2018 American Meteorological Society. For information regarding reuse of this content and general copyright information, consult the [AMS Copyright Policy](#) ([www.ametsoc.org/PUBSReuseLicenses](http://www.ametsoc.org/PUBSReuseLicenses)).

zonal vertical wind shear (ZVWS), the western Pacific subtropical high (WPSH), and the monsoon trough; a similar conclusion was reached by [Chen et al. \(2006\)](#) and [Huangfu et al. \(2017\)](#). [Zhang et al. \(2017\)](#) reproduced the relationship between WNP TC activity and anomalous ZVWS caused by Atlantic meridional mode–induced changes to the Walker circulation. It is found that all four of the abovementioned climate modes—that is, ENSO, ZVWS, WPSH, and the monsoon trough—may be related to the interannual variation of the central equatorial Pacific heating and the subsequent Rossby wave response, and hence may cause the low-level anomalous development of cyclones and/or anticyclones ([Chia and Ropelewski 2002](#)).

Recently, [Zhan et al. \(2011\)](#) and [Ha et al. \(2015\)](#) linked the interannual variability of WNP TC occurrence to the SST in the east Indian Ocean (EIO SST). Two major mechanisms have been proposed to interpret how EIO SST affects the WNP TC genesis. The first is that EIO SST leads to a land–sea thermal contrast, inducing an abnormal East Asian and WNP summer monsoon associated with the monsoon trough, and thus affecting the TC genesis in the region. The second is that the EIO SSTA can excite equatorial Kelvin waves to the east, influencing the surface pressure over the equatorial region and contributing to anomalous anticyclonic (cyclonic) vorticity and divergence (convergence) in the region of concern. Both of these mechanisms result in an anomalous ascending (descending) motion and a wet (dry) midtroposphere, and hence enhance (suppress) the TC genesis in the region ([Ha et al. 2015](#)).

The WNP TC activity has also been connected to the slowly varying Pacific decadal oscillation (PDO; [Liu and Chan 2008](#)) and to the quasi-biennial oscillation (QBO; [Chan 1995a](#)). PDO may contribute to the westward extension and strength of the subtropical high and the midlevel steering flow affecting the TC occurrence pattern ([Liu and Chan 2008](#)). [Camargo and Sobel \(2010\)](#) revisited the issue and found no clear link between the QBO and TC activity.

Although a variety of climate factors, as mentioned above, that modulate the WNP TC activity have been identified, much is yet to be explored in tracing the causal origin of the WNP TC variability. In climate science, time-delayed correlation analysis is still the primary tool for causal identification. This is unfortunate, as there has been strong argument in philosophy against using correlation analysis for this purpose, because, for example, correlation lacks the needed asymmetry or directedness between dynamical events ([Liang 2014](#)). Causality in the modern sense begins with [Granger \(1969\)](#), who formulated the problem as a statistical hypothesis testing, and this approach has been known as the Granger causality test. On the other hand, a new quantity called transfer

entropy (TE; [Schreiber 2000](#)) was empirically proposed, and it has since been of tremendous interest in various disciplines ([Chatzisavvas et al. 2005](#); [Liu et al. 2010](#); [Zhang et al. 2006](#)). It has evolved into alternative forms, such as direct causality entropy ([Duan et al. 2013](#)), transfer zero entropy ([Duan et al. 2014](#)), causation entropy ([Sun and Bollt 2014](#)), etc. Recently, it has been established that Granger causality and transfer entropy 1) are actually equivalent up to a factor of 2, and 2) will give spurious causality inference in several situations; see [Liang \(2016\)](#) for a brief historical review.

During the past years, [Liang \(2008, 2014, 2015, 2016\)](#) realized that causality is actually a real physical notion and can be put on a rigorous footing. In his formalism, causality is measured by information flow (IF). Rigorous formulas have been derived in a closed form, and for linear systems the maximum likelihood estimator of the IF from a series, say,  $X_1$ , to another series,  $X_2$ , turns out to be very simple. IF in this framework is not only very easy to evaluate and efficient for detecting causality for linear systems but proves to be remarkably successful with a highly nonlinear time series that fails TE and the Granger causality test ([Stips et al. 2016](#)). Then [Liang \(2015\)](#) normalized the obtained IF (NIF) in order to assess the relative importance of an identified causality. Unfortunately, the normalization may lead to too-small relative information flows in many situations (a numerical experiment is supplied in [appendix B](#)). An objective of this study is, therefore, to propose a new formula to normalize the IF developed in [Liang \(2014\)](#) so as to fit for our climate–cyclone interactions studies. Another objective regards the prediction of TC activities. The models for this kind of prediction can be broadly divided into two groups: physical models and regression-based methods. For the first group ([Camp et al. 2015](#); [Caron et al. 2011](#); [Chen and Lin 2013](#); [Hsiao et al. 2015](#); [Reale et al. 2014](#); [Strachan et al. 2013](#); [Wang 2012](#); [Zhang et al. 2007](#); [Zhao et al. 2010](#)), equations of mathematical physics and their algorithms are developed to describe and solve the dynamical systems. However, the coarse resolution for the dynamical models often overestimate the size of the tropical storm vortices; computation-intensive complexities always pose a challenge for higher-resolution climate models to implement operational seasonal predictions ([Camp et al. 2015](#)). The second group, which includes linear regressions or Poisson regressions, has been widely used for forecasting TC numbers and variability ([Caron et al. 2015](#); [Chan 1995b](#); [Goh and Chan 2012](#)). However, this method assumes that the observations obey some certain distribution, say, a normal distribution. It is very difficult to obtain a reasonable result for a small sample ([Shenton and Bowman 1977](#)) without any clue about the population shape, which usually is the case in climate science.

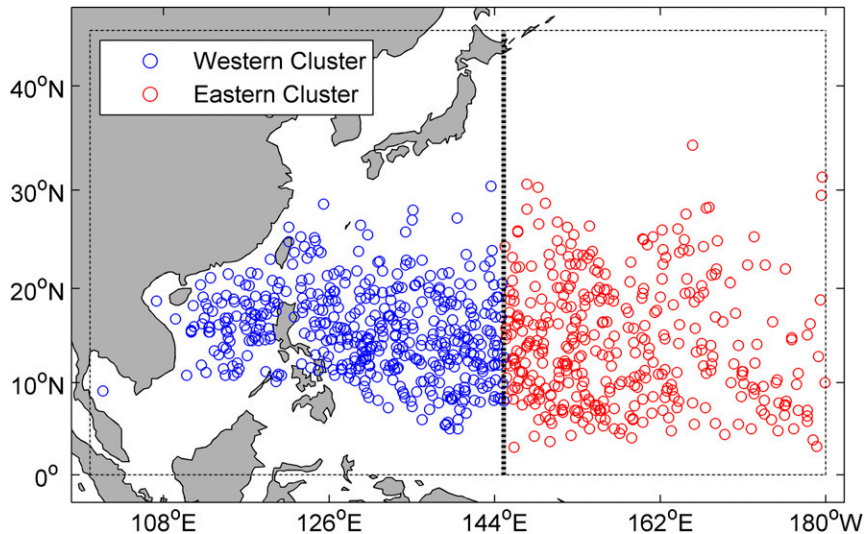


FIG. 1. Positions of TC genesis during the typhoon season for the period 1970–2016 during June–October over the western North Pacific.

The nonparametric Bayesian process (BNP) approach may serve as an acceptable tool for modeling unknown densities. With a BNP model, densities can be estimated without restriction to any specific parameterized form. The Gaussian process prior or the Dirichlet process prior has been commonly used as a BNP prior (Gasparini 1996; Riihimäki and Vehtari 2014). The challenge with the BNP model is its analytical intractability in constructing the prior distribution over scant data (Bai et al. 2017). In this study, we introduce a fuzzy graph approach (Bai et al. 2014) evolved from a new adaptive BNP (BNP-FG) (Bai et al. 2017) to improve the performance of annual WNP TC forecasts with small samples. BNP-FG is mainly based on the traditional Bayesian scheme and the optimal information diffusion model (Wang and You 2002), which is not only an effective method for dealing with the small-sample problem but can capture complex nonlinear relationships without detailed knowledge of the physical processes (Bai et al. 2014, 2015).

The main purpose of this paper is to compare the importance of different climate factors in influencing the WNP TC genesis and to determine the dominant ones using the new normalized IF. The main climate factors are then selected as the input of BNP-FG for a seasonal prediction of WNP TC geneses with rare observations.

The remainder of this paper is organized as follows. Section 2 describes the details of the data used in this paper. To the best of our knowledge, no study reported in the climate literature has used the IF and BNP-FG. Therefore, a section (section 3) is devoted to the introduction of their basics, plus our development in the IF normalization. The results of causality analysis on

cyclone–climate interactions and the annual WNP TC genesis forecast are presented in section 4 and section 5, respectively. This study is concluded in section 6.

## 2. Data

### a. Typhoon data

The quality of the data prior to 1970 has been considered to be poor because of the lack of satellite coverage. We hence select the best-track data of the Joint Typhoon Warning Center ([https://metoc.ndbc.noaa.gov/web/guest/jtwc/best\\_tracks/western-pacific](https://metoc.ndbc.noaa.gov/web/guest/jtwc/best_tracks/western-pacific)) for the period 1970–2016 during June–October over the western North Pacific (0°–45°N, 100°–180°E). The data from the Shanghai Typhoon Institute of China Meteorological Administration (CMA; [www.typhoon.org.cn](http://www.typhoon.org.cn)) and the Regional Specialized Meteorological Center of the Japan Meteorological Agency (JMA; <https://www.jma.go.jp/jma/jma-eng/jma-center/rsmc-hp-pub-eg/trackarchives.html>) are also used as for validation purposes. Only the TCs that have at least tropical storm (TS) intensity (with a maximum sustained wind speed  $V_{\max} \geq 17 \text{ m s}^{-1}$ ) and a lifetime of 48 h or more are considered, in order to minimize the uncertainty in identifying the tropical depression (Liu and Chan 2008) and to address the artificial trend in short-duration storms (Landsea et al. 2010). Moreover, we follow the proposal suggested by Zhan et al. (2011), that is, we divide the WNP into two subregions—a western region west of 145°E and an eastern region east of 145°E—since it displays different trends of TC activity eastward and westward around 145°E. The positions of TC genesis

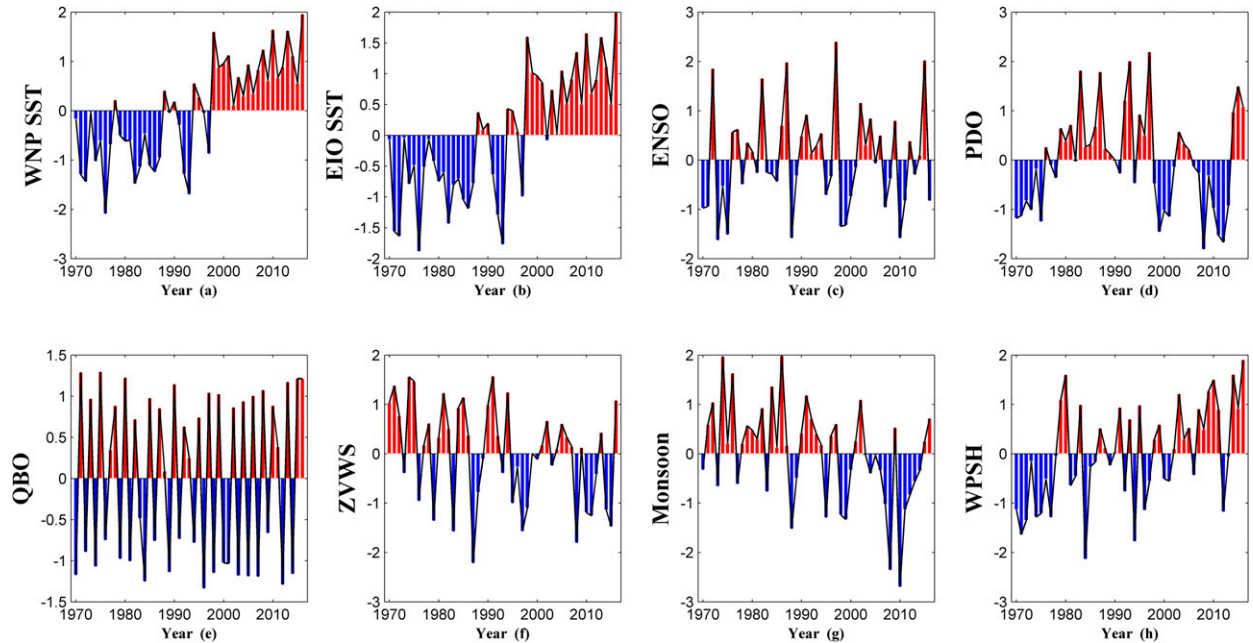


FIG. 2. Normalized time series of various climate indices used in this study: (a) WNP SST, (b) EIO SST, (c) ENSO, (d) PDO, (e) QBO, (f) ZVWS, (g) monsoon, and (h) WPSH.

during typhoon season in the western and eastern clusters are shown in Fig. 1.<sup>1</sup>

### b. Climate data

The climate indices in this study are selected based on the studies mentioned in the introduction. ENSO is characterized by the Niño-3.4 (58°S–58°N, 120°–70°W) index obtained from the NCEP Climate Prediction Center (CPC). Data for PDO are obtained directly from the National Oceanic and Atmospheric Administration (NOAA) Earth System Research Laboratory. In addition, the WNP (0°–45°N, 100°–180°E) and EIO (10°S–22.5°N, 75°–100°E) SST indices are extracted as the average of the Extended Reconstructed SST analyses from NOAA (Smith and Reynolds 2003) measured over the associated region. The definition of the WPSH, as suggested by Hong et al. (2015), is the average grid points of 500-hPa geopotential height > 588 gpm in the range (10°–90°N, 110°–180°E). ZVWS is defined in this paper as the difference in zonal winds between 200 and 850 hPa (Chia and Ropelewski 2002) over the WNP TC genesis region, and the 850-hPa wind composites may characterize the monsoon trough over the WNP (Chia and Ropelewski 2002). The associated wind

data are acquired from the monthly National Centers for Environmental Prediction–National Center for Atmospheric Research reanalysis. Data for QBO are obtained from the University of Berlin by combining observations of the zonal winds at 30 hPa at the three radiosonde stations: Canton Island, Gan/Maldives Islands, and Singapore (Naujokat 1986). All the values of the climate factors for the months of June–October are computed as the averages for each year during 1970–2016 (see Fig. 2). Especially the data for 2007–16 will be used to validate our seasonal forecast.

## 3. Methodologies

### a. Information flow normalization

The climate influence study is mainly based on IF, a physical notion for causality analysis that has just been rigorously formulated. For two time series,  $X_2$  and  $X_1$ , Liang (2014) established that the maximum likelihood estimator of the rate of the IF from  $X_2$  to  $X_1$  is

$$T_{2 \rightarrow 1} = \frac{C_{11}C_{12}C_{2,d1} - C_{12}^2C_{1,d1}}{C_{11}^2C_{22} - C_{11}C_{12}^2}, \quad (1)$$

where  $C_{ij}$  denotes the covariance between  $X_i$  and  $X_j$ , and  $C_{i,dj}$  is determined as follows. Let  $\dot{X}_j$  be the finite-difference approximation of  $dX_j/dt$  using the Euler forward scheme,

<sup>1</sup> If a TC forming on the eastern or western side drops below the TC threshold while propagating westward or eastward and re-intensifies on the western or eastern side, we count it only once and assign it to the eastern or western cluster.

$$\dot{X}_{j,n} = \frac{X_{j,n+k} - X_{j,n}}{k\Delta t},$$

with  $k = 1$  or  $k = 2$  [the details about how to determine  $k$  are referred to in Liang (2014)] and  $\Delta t$  is the time step. Term  $C_{i,dj}$  in Eq. (1) is the covariance between  $X_i$  and  $\dot{X}_j$ . Ideally, if  $T_{2 \rightarrow 1} = 0$ , then  $X_2$  does not cause  $X_1$ ; otherwise, it is causal. In practice, a significance test needs to be done.

An objective here is to find a practical way to normalize the abovementioned IF. As Liang (2015) stated, this may be not as simple as it seems to be. We first need to get back to its original derivation. Given a two-dimensional dynamical system  $d\mathbf{X}/dt = \mathbf{F}(\mathbf{X}, t) + \mathbf{B}(\mathbf{X}, t)\dot{\mathbf{W}}$ , where  $\dot{\mathbf{W}}$  is a 2D vector of white noise, and  $\mathbf{F}$  and  $\mathbf{B}$  can be any nonlinear functions of  $\mathbf{X}$ , Liang (2008) has proved that the rate of change of the marginal entropy  $H_1$  of  $X_1$  is

$$\frac{dH_1}{dt} = -E\left(F_1 \frac{\partial \log \rho_1}{\partial x_1}\right) - \frac{1}{2}E\left(g_{11} \frac{\partial^2 \log \rho_1}{\partial x_1^2}\right), \quad (2)$$

where  $E$  represents mathematical expectation,  $\rho_1$  is the marginal density of  $X_1$ , and  $g_{ij} = \sum_k b_{ik} b_{jk}$ . The first term on the right-hand side of Eq. (2) yields

$$\begin{aligned} -E\left(F_1 \frac{\partial \log \rho_1}{\partial x_1}\right) &= -E\left[\frac{1}{\rho_1} \frac{\partial(F_1 \rho_1)}{\partial x_1} - \frac{\partial F_1}{\partial x_1}\right] \\ &= E\left(\frac{\partial F_1}{\partial x_1}\right) - E\left[\frac{1}{\rho_1} \frac{\partial(F_1 \rho_1)}{\partial x_1}\right]. \end{aligned}$$

Substitution of

$$T_{2 \rightarrow 1} = -E\left[\frac{1}{\rho_1} \frac{\partial(F_1 \rho_1)}{\partial x_1}\right] + \frac{1}{2}E\left(\frac{1}{\rho_1} \frac{\partial^2 g_{11} \rho_1}{\partial x_1^2}\right)$$

(adapted from Liang 2008) into Eq. (2) yields

$$\begin{aligned} \frac{dH_1}{dt} &= E\left(\frac{\partial F_1}{\partial x_1}\right) + T_{2 \rightarrow 1} + \left[-\frac{1}{2}E\left(\frac{1}{\rho_1} \frac{\partial^2 g_{11} \rho_1}{\partial x_1^2}\right) \right. \\ &\quad \left. - \frac{1}{2}E\left(g_{11} \frac{\partial^2 \log \rho_1}{\partial x_1^2}\right)\right]. \end{aligned}$$

The right-hand side has three terms—that is, the change of  $H_1$  due to  $X_1$  itself, the rate of information flow from  $X_2$  to  $X_1$ , and the stochastic effects  $H_1^{\text{noise}}$ —where

$$-\frac{1}{2}E\left(\frac{1}{\rho_1} \frac{\partial^2 g_{11} \rho_1}{\partial x_1^2}\right) - \frac{1}{2}E\left(g_{11} \frac{\partial^2 \log \rho_1}{\partial x_1^2}\right) = \frac{dH_1^{\text{noise}}}{dt}.$$

In the case where  $\mathbf{F} = \mathbf{f} + \mathbf{A}\mathbf{X} + \mathbf{B}\mathbf{B}^T$  with  $\mathbf{f} = (f_1, f_2)^T$ ,  $\mathbf{A} = (a_{ij})_{i,j=1,2}$ , and  $\mathbf{B} = (b_{ij})_{i,j=1,2}$ , which are constant vectors/matrices, the distribution of the state variables will keep being Gaussian, provided that they are originally Gaussian (see Liang 2014). So, we may let

$$\rho_1 = \frac{1}{\sqrt{2\pi}\sigma_1} \exp\left[-\frac{(x_1 - \mu_1)^2}{2\sigma_1^2}\right].$$

It is easy to obtain (Liang 2015)

$$\frac{dH_1^{\text{noise}}}{dt} = \frac{1}{2} \frac{g_{11}}{\sigma_1^2}. \quad (3)$$

We define  $|T_{2 \rightarrow 1}| + |dH_1^{\text{noise}}/dt|$  as the normalizer, which differs from that in Liang (2015) in that the term  $|E(\partial F_1/\partial x_1)|$  is taken out. This makes sense, since that term measures the contribution from  $X_1$  itself and that could be the reason why the resulting relative causality in Liang (2015) is too small. With the modified normalizer,  $T_{2 \rightarrow 1}$  can be normalized as follows:

$$\tau_{2 \rightarrow 1}^B = \frac{\text{abs}(T_{2 \rightarrow 1})}{\text{abs}(T_{2 \rightarrow 1}) + \text{abs}\left(\frac{dH_1^{\text{noise}}}{dt}\right)}. \quad (4)$$

Clearly,  $\tau_{2 \rightarrow 1}^B$  measures the importance of the information flow from  $X_2$  to  $X_1$  in comparison to other stochastic processes. For readers' easy convenience, the step-by-step computation of  $\tau_{2 \rightarrow 1}^B$  is given in algorithm 1 [a matrix laboratory (MATLAB) implementation of algorithm 1 is available online; <https://cn.mathworks.com/matlabcentral/fileexchange/62471-the-normalized-information-flow>]. Moreover, to demonstrate the effectiveness of  $\tau_{2 \rightarrow 1}^B$ , several simulation experiments have been performed in appendix B. Liang's (2015) original IF normalization, written as  $\tau_{2 \rightarrow 1}^L$ , and the normalized transfer entropy (NTE) by Duan et al. (2013) are also included for comparison.

**1) Algorithm 1**

**Input:** Two time series  $X_2$  and  $X_1$ .

**Step 1:** Calculate the rate of information flow  $T_{2 \rightarrow 1}$  from  $X_2$  to  $X_1$  using Eq. (1).

**Step 2:** Estimate the parameters of the two-dimensional dynamical system  $\mathbf{F} = \mathbf{f} + \mathbf{A}\mathbf{X} + \mathbf{B}\mathbf{B}^T$ :

$$a_{11} \approx \frac{C_{22}C_{1,d1} - C_{12}C_{2,d1}}{\det\mathbf{C}}, \quad a_{12} \approx \frac{-C_{12}C_{2,d1} + C_{11}C_{2,d1}}{\det\mathbf{C}}$$

and

$$f_1 \approx E(\dot{X}_1) - a_{11}E(X_1) - a_{12}E(X_2).$$

**Step 3:** Compute the maximum likelihood estimator of  $g_{11}$ :

$$g_{11} \approx \Delta t \cdot E[(\dot{X}_1 - f_1 - a_{11}X_1 - a_{12}X_2)^2].$$

**Step 4:** Substitute  $C_{11}$  for  $\sigma_1^2$ .

**Step 5:** Substitution of  $C_{11}$  and  $g_{11}$  into Eq. (3) yields the rate of the stochastic effect  $\frac{dH_1^{\text{noise}}}{dt}$ .

**Step 6:** Calculate the normalization of  $T_{2 \rightarrow 1}$  based on Eq. (4).

**Output:**  $\tau_{2 \rightarrow 1}^B$ .

*b. Inference using fuzzy graph*

After the main climate factors causing TCs are determined with algorithm 1, a seasonal forecast of TC genesis can be made using BNP-FG (Bai et al. 2017), which is introduced henceforth.

Let  $\mathbf{X} = \{x^{\text{Input}} | x^{\text{Input}} \in \mathbb{R}^\gamma, \text{Input} = 1, \dots, \gamma\}$  and  $\mathbf{Z} = \{z | z \in \mathbb{R}\}$  denote the random variables of interest, where  $\mathbf{X}$  is the input (ENSO and PDO indices, etc.) and  $\mathbf{Z}$  is the output (e.g., seasonal TC number). Let  $(\mathbf{x}^{\text{Input}}, \mathbf{z}) = \{(x_i^{\text{Input}}, z_i) | i = 1, 2, \dots, m\}$  be a set of observations on  $\mathbb{R}^{\gamma+1}$ , where  $\mathbf{x} \subset \mathbf{X}$  and  $\mathbf{z} \subset \mathbf{Z}$ . Suppose that  $U$  and  $V$  are two fuzzy sets of  $\mathbf{X}$  and  $\mathbf{Z}$ , respectively; that is to say,

$$\begin{cases} U = \left[ \frac{\hat{p}_U(x_i^{\text{Input}} | u_a^{\text{Input}})}{u_a^{\text{Input}}}, a = 1, 2, \dots, n_U \right], \\ V = \left[ \frac{\hat{p}_V(z_i | v_b)}{v_b}, b = 1, 2, \dots, n_V \right] \end{cases}$$

where  $\hat{p}_U(x_i^{\text{Input}} | u_a^{\text{Input}})$  and  $\hat{p}_V(z_i | v_b)$  are, respectively, their membership functions in the form of conditional probabilities, with  $(u_a^{\text{Input}}, v_b)$  as an illustrating point. More details are discussed in algorithm 5 of Bai et al. (2017). We can then construct the information gain of  $(u_a^{\text{Input}}, v_b)$  as

$$q_{ab}(x_i^{\text{Input}}, z_i) = \prod_{\text{Input}=1}^{\gamma} \hat{p}_U(x_i^{\text{Input}} | u_a^{\text{Input}}) \cdot \hat{p}_V(z_i | v_b). \quad (5)$$

Let the sum of the information gain be

$$Q_{ab} = \sum_{i=1}^m q_{ab}(x_i^{\text{Input}}, z_i), \quad (6)$$

which consists of the information matrix (Huang 2001)

$$\mathbf{Q} = \begin{matrix} & v_1 & v_2 & \cdots & v_{n_V} \\ \begin{matrix} u_1^1, u_1^2, \dots, u_1^\gamma \\ u_2^1, u_2^2, \dots, u_2^\gamma \\ \vdots \\ u_{n_U}^1, u_{n_U}^2, \dots, u_{n_U}^\gamma \end{matrix} & \begin{pmatrix} Q_{11} & Q_{12} & \cdots & Q_{1n_V} \\ Q_{21} & Q_{22} & \cdots & Q_{2n_V} \\ \vdots & \vdots & \ddots & \vdots \\ Q_{n_U1} & Q_{n_U2} & \cdots & Q_{n_Un_V} \end{pmatrix} \end{matrix}. \quad (7)$$

According to the theory of factor space (Wang 1990), which discusses how to normalize the information matrix appropriately, we use

$$\begin{cases} R = \{r_{ab}\}_{n_U \times n_V} = \{r(u_a^{\text{Input}}, v_b)\}_{n_U \times n_V} \\ r_{ab} = Q_{ab} / s_b \\ s_b = \max_{1 \leq a \leq n_U} Q_{ab} \end{cases} \quad (8)$$

to produce a normalized information matrix, that is, the fuzzy relation matrix  $\mathbf{R}$ ,

$$\mathbf{R} = \begin{matrix} & v_1 & v_2 & \cdots & v_{n_V} \\ \begin{matrix} u_1^1, u_1^2, \dots, u_1^\gamma \\ u_2^1, u_2^2, \dots, u_2^\gamma \\ \vdots \\ u_{n_U}^1, u_{n_U}^2, \dots, u_{n_U}^\gamma \end{matrix} & \begin{pmatrix} r_{11} & r_{12} & \cdots & r_{1n_V} \\ r_{21} & r_{22} & \cdots & r_{2n_V} \\ \vdots & \vdots & \ddots & \vdots \\ r_{n_U1} & r_{n_U2} & \cdots & r_{n_Un_V} \end{pmatrix} \end{matrix}. \quad (9)$$

To calculate the output fuzzy set  $B$ , we first use  $A$  to denote the input fuzzy set

$$s_A(u_a^{\text{Input}}) = \sum_{c=1}^{n_U} \frac{q}{u_c^{\text{Input}}}, \quad q = \begin{cases} 1, c = a \\ 0, c \neq a \end{cases}. \quad (10)$$

Based on the fuzzy inference formula,

$$B = A \circ R_p. \quad (11)$$

Here the operator  $\circ$  signifies the maximum–minimum fuzzy composition rule,

$$s_B(v_b) = \max_{u_a^{\text{Input}} \in U} \{\min[s_A(u_a^{\text{Input}}), r(u_a^{\text{Input}}, v_b)]\}, \quad v_b \in V, \quad (12)$$

where  $r(u_a^{\text{Input}}, v_b) \in (0, 1]$ . Thus, we can obtain

$$s_B(v_b) = \max_{u_a^{\text{Input}} \in U} \{r(u_a^{\text{Input}}, v_b)\}. \quad (13)$$

Finally, the gravity center of the fuzzy set is generated as the output,

$$\tilde{z} = \frac{\sum_{b=1}^{n_V} v_b s_B(v_b)}{\sum_{b=1}^{n_V} s_B(v_b)}. \quad (14)$$

In general, we use the given sample  $(\mathbf{x}, \mathbf{z})$  and illustrating points  $(u_i^a, v_b)$  to construct a relationship between the input and the output in the following form:

$$\begin{aligned} f(x_i^{\text{Input}}, z_i, u_a^{\text{Input}}, v_b) &= \tilde{z}. \\ x_i^{\text{Input}} \in \mathbf{x}, z_i \in \mathbf{z}, a &= 1, 2, \dots, n_U, b = 1, 2, \dots, n_V, \\ \text{If } x_i' &= u_a^{\text{Input}}, \text{ then } z' = \tilde{z}, \end{aligned}$$

where  $x_i'$  represents the values of selected climate indices in a certain year when we want to know its TC genesis number.

TABLE 1. NIF  $\tau_{Col, \rightarrow Row}^B$  between TC genesis number and predictors (%). Boldface font indicates statistically significant values at the 5% level.

$\tau_{Col, \rightarrow Row}^B$	WNP SST	EIO SST	ENSO	PDO	QBO	ZVWS	WPSH	Monsoon
WC	<b>8.743</b>	<b>9.626</b>	<b>26.187</b>	<b>21.604</b>	0.603	<b>1.887</b>	<b>13.949</b>	<b>13.094</b>
EC	<b>7.089</b>	<b>1.212</b>	<b>16.237</b>	<b>13.189</b>	0.306	<b>7.553</b>	<b>11.304</b>	<b>10.297</b>

#### 4. Climate influence on western North Pacific tropical cyclone genesis

We first compute the causal relations between the TC numbers and a variety of climate factors. The whole procedure follows algorithm 1 together with an examination of the statistical significance of the resulting NIF  $\tau_{Col, \rightarrow Row}^B$  (i.e., if  $\tau_{Col, \rightarrow Row}^B \geq 1\%$ , and if the IF is significant at the 5% confidence level; Liang 2015). The results are tabulated in Table 1. This section is a summary of the results. Note that the direction of the causality or information flow in the table is from the column index to the row index.

As is clearly seen, most of the NIFs are significant (as highlighted) except QBO, which generally agrees with previous studies mentioned in the literature. For the western cluster (WC) time series—that is, the first row in Table 1—the NIF values vary from 0.3605% to 26.1865%. The maximum is  $\tau_{ENSO \rightarrow CITC}^B$ , in agreement with Chia and Ropelewski (2002), who claimed that ENSO is a major factor in determining the seasonal TC mean genesis positions. Second to it is  $\tau_{PDO \rightarrow CITC}^B$ . This is consistent with Liu and Chan (2008), who found that PDO displays a dipole-like structure on the 500-hPa geopotential height anomaly map. Strong easterly anomalies tend to steer TCs toward the west.

From the second row of the table, the variability in the eastern cluster (EC) seems to be largely tied to, aside from ENSO and PDO, WPSH. WPSH generally moves northward in June, reaching its northernmost position near 40°N in August and September, and withdraws in October. When it retreats from the South China Sea (SCS), the monsoon westerly winds penetrate from the Indian Ocean to the SCS, the Philippine Sea, and the western Pacific, which may be more favorable for TC genesis over the WNP (Frank 1987). The most interesting information is found in the last two columns of Table 1. These values validate the work of Chia and Ropelewski (2002), who showed that the strengthened (weakened) WPSH and the enhanced (reduced) monsoon trough in the Philippine Sea lead to an eastward (westward) displacement of the major TC genesis pattern; this is also consistent with the ENSO composites of Wang (1995).

Because climate science correlation analysis may be a primary approach for causality detecting, we also compute the correlation coefficients between the pairs for comparison

purposes. The results are shown in Table 2. Most of the results are not significant, except those with ENSO and PDO. This suggests that correlation analysis should not be a prior choice for predictor selection in climate science. In other words, although correlation analysis may help select the proper climate factors with the largest correlation coefficients, it cannot display the inner links between some certain climate indices and the WNP TCs. For example, the WNP SST should be an important climate index for influencing TCs over the WNP; however, correlation analysis cannot always correctly validate it (see Table 2). In contrast, at the same statistical significance level, we can obtain the cause–effect relation between the events of interest using the new NIF without computational complexity.

#### 5. Prediction of annual TC activity over the WNP

To achieve acceptable prediction performance, we first get two ranking lists of climate indices ordered by the values of NIF and correlation coefficients based on Tables 1 and 2, respectively. Then, as recommended by Song et al. (2013), we select Top- $k$  factors from the two ranking lists, where  $k = \sqrt{m} \cdot \log m$  and  $m$  is the number of potentially selected indices. In this study the number of climate factors is eight, then  $k = 5$ . Thus, the common indices in the two Top- $k$  ranking lists are chosen as the final predictors. Following this procedure, ENSO, PDO, and WPSH are the three most important predictors causing TCs in the western cluster; ENSO, PDO, and monsoons are the major ones for the eastern cluster. Therefore, in this section, we analyze the prediction capability of BNP-FG in coordination with these selected climate influences and compare it with the Poisson regression, which is a common approach in climatology.

##### a. Experiment 1: Prediction of the annual TC genesis in the eastern region of the WNP

Following a general rule for forecasting exercises, 80% of the sample is used for training and the rest is used for validation. Therefore, we train BNP-FG with data from 1970 to 2006 and make predictions from 2007 to 2016 (it should be noticed that the size of the sample is small). A new framework is presented here to illustrate the step-by-step implementation of BNP-FG.

TABLE 2. Correlation  $R$  between TC genesis number and predictors. Boldface font indicates statistically significant values at the 5% level.

$R$	WNP SST	EIO SST	ENSO	PDO	QBO	ZVWS	WPSH	Monsoon
WC	16.632	18.654	<b>-62.906</b>	<b>-52.519</b>	3.237	<b>34.182</b>	-23.249	<b>-41.529</b>
EC	-23.100	<b>-29.206</b>	<b>50.441</b>	<b>49.199</b>	-3.415	11.733	<b>44.555</b>	-11.082

Step 1: Let the indices of ENSO, PDO, and WPSH, and the recorded TC genesis numbers measured from 1970 to 2006 be

$$(\mathbf{x}^{\text{Input}}, \mathbf{z}) = \{(x_i^1, x_i^2, x_i^3, z_i) | (-1.0, 1.0, -0.3, 9), \dots, (-0.9, 1.4, 0.5677, 12), \dots\}.$$

Step 2: According to the maximum and minimum values of  $\mathbf{x}^{\text{Input}}$  and  $\mathbf{z}$  in Fig. 2, let the illustrating points  $(u_a^{\text{Input}}, v_b)$  be

$$\left\{ \begin{array}{l} \{u_a^1 | u_a^1 = -1.6: \text{step: } 2.2, \text{ step} = 0.1, a = 1, 2, \dots, 39\} \\ \{u_a^2 | u_a^2 = -2.2: \text{step: } 1.3, \text{ step} = 0.1, a = 1, 2, \dots, 36\} \\ \{u_a^3 | u_a^3 = -2.7: \text{step: } 1.8, \text{ step} = 0.1, a = 1, 2, \dots, 46\} \\ \{v_b | v_b = 0: \text{step: } 15, \text{ step} = 1, b = 1, 2, \dots, 16\} \end{array} \right.$$

Step 3: Based on algorithm 5 of Bai et al. (2017), the membership functions  $\hat{p}_U(x_i^{\text{Input}} | u_a^{\text{Input}})$  and  $\hat{p}_V(z_i | v_b)$  can be computed.

Step 4: Then, the fuzzy relationship matrix  $\mathbf{R}$  can be computed using Eqs. (5)–(9).

Step 5: Recalling Eqs. (10)–(14), the TC genesis number in response to every possible  $\mathbf{x}^{\text{Input}}$  can be inferred. We take the prediction for year

2016 as an example. We know that  $(x_{2016-1970+1=47}^1 \approx -0.8, x_{47}^2 \approx 1.1, x_{47}^3 \approx 0.7)$  in 2015 from Fig. 2. We use Eq. (12) to obtain

$$s_A[(-0.8, 1.1, 0.7)] = \frac{0}{(-1.6, -2.2, -2.7)} + \dots + \frac{1}{(-0.8, 1.1, 0.7)} + \dots + \frac{0}{(2.2, 1.3, 1.8)}.$$

Next, based on the

$$\text{Num} = [0.7 - (-2.7)]/0.1 \times 36 \times 39 + [1.1 - (-2.2)]/0.1 \times 39 + [-0.8 - (-1.6)]/0.1 + 1 = 49\,032$$

-th row of  $\mathbf{R}$  and Eq. (13), we compute

$$s_B(v_b) = \frac{1.0970e^{-4}}{0} + \frac{0.0029}{1} + \frac{0.0197}{2} + \dots + \frac{0.4716}{14} + \frac{0.4410}{15}.$$

Finally, we calculate the gravity center of the output fuzzy set as the predicted value using Eq. (14),

$$\begin{aligned} \tilde{z} &= \frac{1.0960e^{-4} \times 0 + 0.0029 \times 1 + 0.0197 \times 2 + \dots + 0.4716 \times 14 + 0.4410 \times 15}{1.0960e^{-4} + 0.0029 + 0.0197 + \dots + 0.4716 + 0.4410} \\ &= 10.3085, \end{aligned}$$

which is nearly the same as the true number of TC genesis in 2016 (see Fig. 3a).

Following the steps given above, the results of BNP-FG for TC genesis forecasting over the WNP can be obtained (see Fig. 3a). Figure 3a shows that BNP-FG can capture the decreasing trend in 2007–08, the increase in 2008–09, the drop in 2010, the increasing pattern in 2011–15, and the drop in 2016. The mean absolute percentage error (MAPE; Caron et al. 2015) and the root-mean-square error (RMSE; Caron et al. 2015) are also employed as objective functions to calibrate the new model (see Table 3). It should be noted that in this section we discuss the results based on only the JTWC best-track data. Obviously, the BNP-FG

performs rather satisfactorily, with an MAPE value of 19.05% and an RMSE value of 1.5233. One of the most common models to estimate the relation between objects of interest in climate science is Poisson regression (PR). We hence also perform PR for comparison. We use the “glmfit” and “glmval” functions in the toolbox of MATLAB to obtain the prediction of TC genesis numbers in 2007–16. The results are displayed in Fig. 3a. From the figure it is obvious that BNP-FG performs better than PR: BNP-FG outperforms PR by about 21.35% and 9.32% in terms of MAPE and RMSE reductions, respectively. This may be attributed to samples containing insufficient information for PR to model the interannual variability of TC geneses.

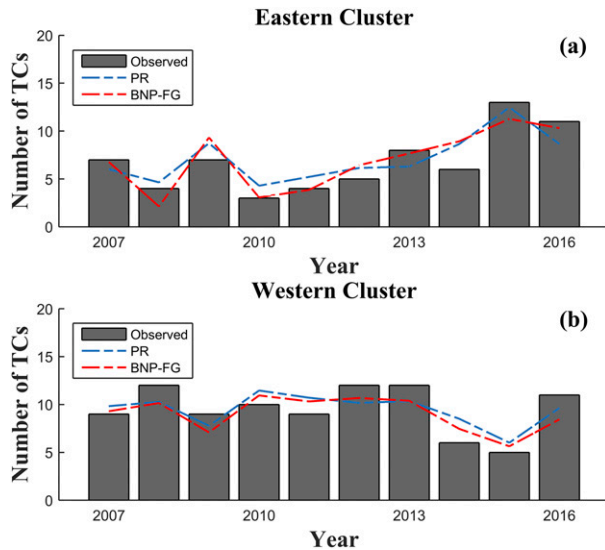


FIG. 3. Seasonal forecasts for (a) eastern and (b) western clusters during the 2007–16 period. Shown are PR (blue) and BNP-FG (red).

*b. Experiment 2: Prediction of the interannual TC genesis in the western region of the WNP*

As in experiment 1, in step 1 the ENSO, PDO, and monsoon indices and the TC numbers in the eastern cluster are selected as the input. Figure 3b shows the observed and reconstructed TC number using different models. Clearly BNP-FG still provides better predictions than PR, with the best MAPE and RMSE reductions by 14.53% and 1.5224, respectively. From this we see a strong prospect for the prediction of the interannual variability of the WNP TC numbers from limited information using BNP-FG.

*c. Experiment 3: Prediction of the interannual TC genesis in the whole WNP using data from CMA and JMA*

In this experiment we repeat the abovementioned procedures using the data from CMA and JMA. The results are presented in the supplementary material (Tables S1–S4). We take the prediction of TC genesis frequency for the WC based on the JMA datasets as an example. First, we get two ranking lists of climate indices ordered by the values of NIF and correlation coefficients based on Tables S1 and S2, respectively. Then, we select Top-*k* factors from the two ranking lists, where *k* = 5. The Top-*k* influences derived from Table S1 are ENSO, PDO, WNP SST, WPSH, and EIO SST. The Top-*k* list from Table S2 only consists of ENSO, PDO, and WPSH, since other factors’ correlations with TC genesis for WC are insignificant at the 5% level. Thus, the common indices in the two Top-*k* ranking lists are ENSO, PDO, and WPSH as final predictors. The performances of

TABLE 3. Skill scores (in terms of MAPE and RMSE) of different models for the ECs and WCs of the WNP (boldface font indicates the best performance).

Datasets		PR		BNP-FG	
		WC	EC	WC	EC
JTWC	MAPE	0.174	0.242	<b>0.149</b>	<b>0.191</b>
	RMSE	1.596	1.680	<b>1.522</b>	<b>1.523</b>
CMA	MAPE	0.223	0.233	<b>0.209</b>	<b>0.209</b>
	RMSE	2.473	1.380	<b>2.436</b>	<b>1.272</b>
JMA	MAPE	0.165	0.311	<b>0.145</b>	<b>0.227</b>
	RMSE	2.332	2.577	<b>2.286</b>	<b>2.080</b>

BNP-FG versus PR over the years 2007–16 for WC using the selected predictors are shown in Fig. S1. Subsequent to this example, we can obtain the results of predicting TC genesis frequency for different regions over the WNP based on JMA and CMA datasets (see Figs. S2–S4). Details about the robustness analyses are provided in Table 3. Although there are some discrepancies between the selected predictors derived from different datasets (it may be attributed to different physical parameterization schemes and data assimilation techniques utilized by the operational centers in TC activity forecasting; Peng et al. 2017), the same conclusion can be drawn from Table 3; that is to say, the proposed algorithm mentioned above makes a competitive tool for forecasting the number of WNP TCs when measurements are insufficient.

**6. Conclusions**

In this study we introduced a recently formulated rigorous causality inference method—that is, the information flow analysis method by Liang (2014)—into the field of climate–cyclone interaction analysis and TC forecasting, and developed for it a new normalization scheme. We used the NIF to identify the cause–effect relation between the western North Pacific tropical cyclone genesis and a variety of climate indices. Key factors are then selected for seasonal prediction. The resulting causalities generally agree with previous studies on the variability of the WNP TC genesis, but they show a difference from those obtained through correlation analysis, a technique most commonly used in climate science. Although there are no significant correlations between certain climate factors and TCs over the WNP, with the new method the links between them can be accurately revealed. In particular, the principal influences of ENSO and PDO on the WNP TC variability have been reconfirmed through the causality analysis; the secondary influences of WPSH and monsoon trough have been faithfully detected as well, consistent with the observation that they significantly affect the atmospheric

circulation and result in atmospheric anomalies over the WNP (Chia and Ropelewski 2002; Xie et al. 2009; Zhan et al. 2011).

The second part of this study is the prediction of the interannual variability of the TC numbers. Based on a fuzzy graph that evolved from a new nonparametric Bayesian process (BNP-FG), a robust model was proposed for predicting the TC numbers in the western and eastern regions over the WNP when the observations are insufficient. The causal climate factors selected through the aforementioned causality analysis are taken as input for the prediction. It has been shown that the prediction with the ENSO, PDO, and WPSH indices can achieve acceptable performance for the western cluster; for the eastern cluster, the prediction with ENSO, PDO, and monsoon taken into account is satisfactory. A classic Poisson regression (PR) is also employed for comparison. It is observed that the new method significantly outperforms PR. Although much is yet to be improved, this newly proposed method—that is, the BNP-FG model combined with the recently developed causality analysis—provides a competitive tool for more reliable TC genesis forecasts. We look forward to seeing more applications in the future over the different basins.

*Acknowledgments.* The authors are very grateful to the anonymous editor and reviewers for their valuable comments and constructive suggestions, which helped us to improve significantly the quality of the paper. XSL acknowledges the supports from the 2015 Jiangsu Program for Innovation Research and Entrepreneurship Groups, and the National Program on Global Change and Air-Sea Interaction (GASI-IPOVAI-06). This research was supported by the National Natural Science Foundation of China (51609254) and the Specific Fund for the Industrial Site in the city of Tangshan (CQZ-2014001).

## APPENDIX A

### Glossary of the Acronyms

BNP	Nonparametric Bayesian process
CMA	China Meteorological Administration
CPC	Climate Prediction Center
EC	Eastern cluster
EIO	East Indian Ocean
ENSO	El Niño–Southern Oscillation

FG	Fuzzy graph
IF	Information flow
JMA	Japan Meteorological Agency
MAPE	Mean absolute percentage error
MATLAB	Matrix laboratory
NIF	Normalized information flow
NOAA	National Oceanic and Atmospheric Administration
NTE	Normalized transfer entropy
PDO	Pacific decadal oscillation
PR	Poisson regression
QBO	Quasi-biennial oscillation
RMSE	Root-mean-square error
SCS	South China Sea
SST	Sea surface temperature
TC	Tropical cyclone
TE	Transfer entropy
TS	Tropical storm
WC	Western cluster
WNP	Western North Pacific
WPSH	Western Pacific subtropical high
ZVWS	Zonal vertical wind shear

## APPENDIX B

### Several Numerical Simulations

In this section two numerical examples (adapted from Duan et al. 2013) are adopted to validate  $\tau_{2 \rightarrow 1}^B$ . A comparison with the NTE (Duan et al. 2013) and  $\tau_{2 \rightarrow 1}^L$  (Liang 2015) is also presented.

TABLE B1. NTE, NIF<sup>L</sup>, and NIF<sup>B</sup> for Eq. (B1).

	NTE	NIF <sup>L</sup>	NIF <sup>B</sup>
$x \rightarrow y$	0.348	0.000	0.000
$y \rightarrow x$	0.055	0.000	0.000
$x \rightarrow z$	0.409	0.006	0.698
$z \rightarrow x$	0.058	0.000	0.000
$z \rightarrow y$	0.393	0.172	0.975
$y \rightarrow z$	0.044	0.001	0.003

TABLE B2. NTE, NIF<sup>L</sup>, and NIF<sup>B</sup> for Eq. (B2).

	NTE	NIF <sup>L</sup>	NIF <sup>B</sup>
$x \rightarrow y$	0.274	0.009	0.367
$y \rightarrow x$	0.000	0.000	0.000
$x \rightarrow z$	0.623	0.011	0.633
$z \rightarrow x$	0.000	0.000	0.000
$z \rightarrow y$	0.308	0.109	0.285
$y \rightarrow z$	0.048	0.000	0.008

Experiment 1: Linear equations

$$\begin{cases} z_{k+1} = 0.8x_k + 0.2z_k + v_{1k}, \\ y_{k+1} = 0.6z_k + v_{2k} \end{cases}, \quad (B1)$$

where  $x_k \sim N(0, 1)$ ,  $v_{1k}, v_{2k} \sim N(0, 1)$ , and  $z_0 = 3.2$ . We have run 6000 steps, but the initial 3000 are discarded to obtain two stationary series. The NIF and NTE between each pair of  $x, y$ , and  $z$  are then computed and listed in Table B1. Based on the NIF values, it can be seen that  $x$  causes  $z$  and  $z$  causes  $y$  because  $\tau_{x \rightarrow z}^B = 0.698$  and  $\tau_{z \rightarrow y}^B = 0.975$  are much larger than zero. This conclusion is obviously consistent with Eq. (B1) from which it can be seen that there is information delivery from both  $x$  to  $z$  and  $z$  to  $y$ . Although  $\tau_{z \rightarrow y}^L = 0.172$  can correctly unravel the causal relation between  $z$  and  $y$ , it is hard to detect the information flow pathway from  $x$  to  $z$  from  $\tau_{x \rightarrow z}^L = 0.006$ .

In addition, based on Eq. (19) from (Duan et al. 2013), it is noticed that NIT can achieve nearly the same performance with ours (except for  $NTE_{x \rightarrow y}$ , because NIF represents a direct cause-effect relation, while NTE cannot distinguish whether the causality is direct or indirect). But as Duan et al. (2013) stated, the computational complexity for NTE is  $O[N^2(k_1 + l_1)^2]$ , where  $N$  represents the sample size, and  $k_1$  and  $l_1$  are the embedding dimensions of each pair of objects. In contrast, the computational complexity for NIF is only  $O(N)$ , by far lower than that for NTE.

Experiment 2: Nonlinear equations

$$\begin{cases} z_{k+1} = 1 - 2|0.5 - (0.8x_k + 0.4\sqrt{z_k}) + v_{1k}| \\ y_{k+1} = 5(z_k + 7.2)^2 + 10\sqrt{|x_k|} + v_{2k} \end{cases}, \quad (B2)$$

where  $x_k \sim U(4, 5)$ ,  $v_{1k}, v_{2k} \sim N(0, 0.05)$ , and  $z_0 = 0.2$ . Following Eq. (B1), we compute all the values of NTE and NIF, and list them in Table B2. Clearly, our NIF here yields good results, considering the preset information flow pathways in Eq. (B2). Its performance is obviously better than that of Liang (2015) and NTE (Duan et al. 2013). Our normalization scheme for Liang’s (2014) IF is hence successful.

REFERENCES

Bai, C., M. Hong, D. Wang, R. Zhang, and L. Qian, 2014: Evolving an information diffusion model using a genetic algorithm for monthly river discharge time series interpolation and forecasting. *J. Hydrometeor.*, **15**, 2236–2249, <https://doi.org/10.1175/JHM-D-13-0184.1>.

—, R. Zhang, M. Hong, L. Qian, and Z. Wang, 2015: A new information diffusion modelling technique based on vibrating string equation and its application in natural disaster risk assessment. *Int. J. Gen. Syst.*, **44**, 601–614, <https://doi.org/10.1080/03081079.2014.980242>.

—, —, L. Qian, and Y. Wu, 2017: A fuzzy graph evolved by a new adaptive Bayesian framework and its applications in natural hazards. *Nat. Hazards*, **87**, 899–918. <https://doi.org/10.1007/s11069-017-2801-y>.

Camargo, S. J., and A. H. Sobel, 2010: Revisiting the influence of the quasi-biennial oscillation on tropical cyclone activity. *J. Climate*, **23**, 5810–5825, <https://doi.org/10.1175/2010JCLI3575.1>.

Camp, J., M. Roberts, C. MacLachlan, E. Wallace, L. Hermanson, A. Brookshaw, A. Arribas, and A. A. Scaife, 2015: Seasonal forecasting of tropical storms using the Met Office GloSea5 seasonal forecast system. *Quart. J. Roy. Meteor. Soc.*, **141**, 2206–2219, <https://doi.org/10.1002/qj.2516>.

Caron, L. P., C. G. Jones, and K. Winger, 2011: Impact of resolution and downscaling technique in simulating recent Atlantic tropical cyclone activity. *Climate Dyn.*, **37**, 869–892, <https://doi.org/10.1007/s00382-010-0846-7>.

—, M. Boudreault, and S. J. Camargo, 2015: On the variability and predictability of eastern Pacific tropical cyclone activity. *J. Climate*, **28**, 9678–9696, <https://doi.org/10.1175/JCLI-D-15-0377.1>.

Chan, J. C. L., 1995a: Tropical cyclone activity in the western North Pacific in relation to the stratospheric quasi-biennial oscillation. *Mon. Wea. Rev.*, **123**, 2567–2571, [https://doi.org/10.1175/1520-0493\(1995\)123<2567:TCAITW>2.0.CO;2](https://doi.org/10.1175/1520-0493(1995)123<2567:TCAITW>2.0.CO;2).

—, 1995b: Prediction of annual tropical cyclone activity over the western North Pacific and the South China Sea. *Int. J. Climatol.*, **15**, 1011–1019, <https://doi.org/10.1002/joc.3370150907>.

Chatzisavvas, K. Ch., Ch. C. Moustakidis, and C. P. Panos, 2005: Information entropy, information distances, and complexity in atoms. *J. Chem. Phys.*, **123**, 174111–174121, <https://doi.org/10.1063/1.2121610>.

Chen, J. H., and S. J. Lin, 2013: Seasonal predictions of tropical cyclones using a 25-km-resolution general circulation model. *J. Climate*, **26**, 380–398, <https://doi.org/10.1175/JCLI-D-12-00061.1>.

Chen, T. C., S. Y. Wang, and M. C. Yen, 2006: Interannual variation of the tropical cyclone activity over the western North Pacific. *J. Climate*, **19**, 5709, <https://doi.org/10.1175/JCLI3934.1>.

- Chia, H. H., and C. F. Ropelewski, 2002: The interannual variability in the genesis location of tropical cyclones in the northwest Pacific. *J. Climate*, **15**, 2934–2944, [https://doi.org/10.1175/1520-0442\(2002\)015<2934:TIVITG>2.0.CO;2](https://doi.org/10.1175/1520-0442(2002)015<2934:TIVITG>2.0.CO;2).
- Duan, P., F. Yang, T. Chen, and S. L. Shah, 2013: Direct causality detection via the transfer entropy approach. *IEEE Trans. Control Syst. Technol.*, **21**, 2052–2066, <https://doi.org/10.1109/TCST.2012.2233476>.
- , —, S. L. Shah, and T. Chen, 2014: Transfer zero-entropy and its application for capturing cause and effect relationship between variables. *IEEE Trans. Control Syst. Technol.*, **23**, 855–867, <https://doi.org/10.1109/tcst.2014.2345095>.
- Frank, W. M., 1987: Tropical cyclone formation. *A Global View of Tropical Cyclone*, R. L. Elsberry et al., Eds., Naval Postgraduate School, 53–90.
- Gasparini, M., 1996: Bayesian density estimation via Dirichlet density processes. *J. Nonparametric Stat.*, **6**, 355–366, <https://doi.org/10.1080/10485259608832681>.
- Goh, Z. C., and J. C. L. Chan, 2012: Variations and prediction of the annual number of tropical cyclones affecting Korea and Japan. *Int. J. Climatol.*, **32**, 178–189, <https://doi.org/10.1002/joc.2258>.
- Granger, C. W. J., 1969: Investigating causal relations by econometric models and cross-spectral methods. *Econometrica*, **37**, 424–438, <https://doi.org/10.2307/1912791>.
- Gray, W. M., 1998: The formation of tropical cyclones. *Meteor. Atmos. Phys.*, **67**, 37–69, <https://doi.org/10.1007/BF01277501>.
- Ha, Y., Z. Zhong, X. Yang, and Y. Sun, 2015: Contribution of East Indian Ocean SSTA to Western North Pacific tropical cyclone activity under El Niño/La Niña conditions. *Int. J. Climatol.*, **35**, 506–519, <https://doi.org/10.1002/joc.3997>.
- Hong, M., R. Zhang, C. Z. Bai, X. Chen, D. Wang, and J. Ge, 2015: Reconstruction of statistical–dynamical model of the Western Pacific subtropical high and East Asian summer monsoon factors and its forecast experiments. *Nat. Hazards*, **75**, 2863–2883, <https://doi.org/10.1007/s11069-014-1467-y>.
- Hsiao, L. F., and Coauthors, 2015: Blending of global and regional analyses with a spatial filter: Application to typhoon prediction over the western North Pacific Ocean. *Wea. Forecasting*, **30**, 754–770, <https://doi.org/10.1175/WAF-D-14-00047.1>.
- Huang, C., 2001: Information matrix and application. *Int. J. Gen. Syst.*, **30**, 603–622, <https://doi.org/10.1080/03081070108960737>.
- Huangfu, J., R. Huang, W. Chen, T. Feng, and L. Wu, 2017: Interdecadal variation of tropical cyclone genesis and its relationship to the monsoon trough over the western North Pacific. *Int. J. Climatol.*, **37**, 3587–3596, doi:10.1002/joc.4939.
- Landsea, C. W., G. A. Vecchi, L. Bengtsson, and T. R. Knutson, 2010: Impact of duration thresholds on Atlantic tropical cyclone counts. *J. Climate*, **23**, 2508–2519, <https://doi.org/10.1175/2009JCLI3034.1>.
- Liang, X. S., 2008: Information flow within stochastic dynamical systems. *Phys. Rev.*, **78E**, 031113, <https://doi.org/10.1103/PhysRevE.78.031113>.
- , 2014: Unraveling the cause-effect relation between time series. *Phys. Rev.*, **90E**, 052150, <https://doi.org/10.1103/PhysRevE.90.052150>.
- , 2015: Normalizing the causality between time series. *Phys. Rev.*, **92E**, 022126, <https://doi.org/10.1103/PhysRevE.92.022126>.
- , 2016: Information flow and causality as rigorous notions *ab initio*. *Phys. Rev.*, **94E**, 052201, <https://doi.org/10.1103/PhysRevE.94.052201>.
- Liu, K. S., and J. C. L. Chan, 2008: Interdecadal variability of western North Pacific tropical cyclone tracks. *J. Climate*, **21**, 4464–4476, <https://doi.org/10.1175/2008JCLI2207.1>.
- Liu, L., J. Zhou, X. An, Y. Zhang, and L. Yang, 2010: Using fuzzy theory and information entropy for water quality assessment in Three Gorges region, China. *Expert Syst. Appl.*, **37**, 2517–2521, <https://doi.org/10.1016/j.eswa.2009.08.004>.
- Naujokat, B., 1986: An update of the observed quasi-biennial oscillation of the stratospheric winds over the tropics. *J. Atmos. Sci.*, **43**, 1873–1880, [https://doi.org/10.1175/1520-0469\(1986\)043<1873:AUOTOQ>2.0.CO;2](https://doi.org/10.1175/1520-0469(1986)043<1873:AUOTOQ>2.0.CO;2).
- Peng, X., J. Fei, X. Huang, and X. Cheng, 2017: Evaluation and error analysis of official forecasts of tropical cyclones during 2005–14 over the western North Pacific. Part I: Storm tracks. *Wea. Forecasting*, **32**, 689–712, <https://doi.org/10.1175/WAF-D-16-0043.1>.
- Reale, O., K. M. Lau, A. Silva, and T. Matsui, 2014: Impact of assimilated and interactive aerosol on tropical cyclogenesis. *Geophys. Res. Lett.*, **41**, 3282–3288, <https://doi.org/10.1002/2014GL059918>.
- Riihimäki, J., and A. Vehtari, 2014: Laplace approximation for logistic Gaussian process density estimation and regression. *Bayesian Anal.*, **9**, 425–448, <https://doi.org/10.1214/14-BA872>.
- Schreiber, T., 2000: Measuring information transfer. *Phys. Rev. Lett.*, **85**, 461–464, <https://doi.org/10.1103/PhysRevLett.85.461>.
- Shenton, L. R., and K. O. Bowman, 1977: Maximum likelihood estimation in small samples. *Tien Tzu Hsueh Pao*, **32**, 2020–2023.
- Smith, T. M., and R. W. Reynolds, 2003: Extended reconstruction of global sea surface temperatures based on COADS data (1854–1997). *J. Climate*, **16**, 1495–1510, <https://doi.org/10.1175/1520-0442-16.10.1495>.
- Song, Q., J. Ni, and G. Wang, 2013: A fast clustering-based feature subset selection algorithm for high-dimensional data. *IEEE Trans. Knowl. Data Eng.*, **25**, 1–14, <https://doi.org/10.1109/TKDE.2011.181>.
- Stips, A., D. Macias, C. Coughlan, E. Garcigorri, and X. S. Liang, 2016: On the causal structure between CO<sub>2</sub> and global temperature. *Sci. Rep.*, **6**, 21 691, <https://doi.org/10.1038/srep21691>.
- Strachan, J., P. L. Vidale, K. Hodges, M. Roberts, and M. E. Demory, 2013: Investigating global tropical cyclone activity with a hierarchy of AGCMs: The role of model resolution. *J. Climate*, **26**, 133–152, <https://doi.org/10.1175/JCLI-D-12-00012.1>.
- Sun, J., and E. M. Bollt, 2014: Causation entropy identifies indirect influences, dominance of neighbors and anticipatory couplings. *Physica D*, **267**, 49–57, <https://doi.org/10.1016/j.physd.2013.07.001>.
- Wang, B., 1995: Interdecadal changes in El Niño onset in the last four decades. *J. Climate*, **8**, 267–285, [https://doi.org/10.1175/1520-0442\(1995\)008<0267:ICIENO>2.0.CO;2](https://doi.org/10.1175/1520-0442(1995)008<0267:ICIENO>2.0.CO;2).
- , and J. C. L. Chan, 2002: How strong ENSO events affect tropical storm activity over the western North Pacific. *J. Climate*, **15**, 1643–1658, [https://doi.org/10.1175/1520-0442\(2002\)015<1643:HSEAT>2.0.CO;2](https://doi.org/10.1175/1520-0442(2002)015<1643:HSEAT>2.0.CO;2).
- Wang, P.-Z., 1990: A factor spaces approach to knowledge representation. *Fuzzy Sets Syst.*, **36**, 113–124, [https://doi.org/10.1016/0165-0114\(90\)90085-K](https://doi.org/10.1016/0165-0114(90)90085-K).
- Wang, X., and Y. You, 2002: The theory of optimal information diffusion estimation and its application. *Computational Intelligent Systems for Applied Research: Proceedings of the Fifth International FLINS Conference*, D. Ruan, P. D’Hondt, and E. E. Kerre, Eds., 198–207, [https://doi.org/10.1142/9789812777102\\_0025](https://doi.org/10.1142/9789812777102_0025).

- Wang, Y., 2012: Recent research progress on tropical cyclone structure and intensity. *Trop. Cyclone Res. Rev.*, **1**, 254–275, <https://doi.org/10.6057/2012TCRR02.05>.
- Xie, S.-P., K. M. Hu, J. Hafner, H. Tokinaga, Y. Du, G. Huang, and T. Sampe, 2009: Indian Ocean capacitor effect on Indo-western Pacific climate during the summer following El Niño. *J. Climate*, **22**, 730–747, <https://doi.org/10.1175/2008JCLI2544.1>.
- Zhan, R., Y. Wang, and X. Lei, 2011: Contributions of ENSO and east Indian Ocean SSTA to the interannual variability of northwest Pacific tropical cyclone frequency. *J. Climate*, **24**, 509–521, <https://doi.org/10.1175/2010JCLI3808.1>.
- Zhang, W., G. A. Vecchi, G. Villarini, H. Murakami, A. Rosati, X. Yang, L. Jia, and F. Zeng, 2017: Modulation of western North Pacific tropical cyclone activity by the Atlantic Meridional Mode. *Climate Dyn.*, **48**, 631–647, <https://doi.org/10.1007/s00382-016-3099-2>.
- Zhang, X., Q. Xiao, and P. J. Fitzpatrick, 2007: The impact of multisatellite data on the initialization and simulation of Hurricane Lili's (2002) rapid weakening phase. *Mon. Wea. Rev.*, **135**, 526–548, <https://doi.org/10.1175/MWR3287.1>.
- Zhang, Y., Z. Yang, and W. Li, 2006: Analyses of urban ecosystem based on information entropy. *Ecol. Modell.*, **197**, 1–12, <https://doi.org/10.1016/j.ecolmodel.2006.02.032>.
- Zhao, M., I. M. Held, and G. A. Vecchi, 2010: Retrospective forecasts of the hurricane season using a global atmospheric model assuming persistence of SST anomalies. *Mon. Wea. Rev.*, **138**, 3858–3868, <https://doi.org/10.1175/2010MWR3366.1>.